NASA Technical Memorandum 86754

Effect of Ground and/or Ceiling Planes on Thrust of Rotors in Hover

Vernon J. Rossow

July 1985

National Aeronautics and
Space Administration

NASA Technical Memorandum 86754

Effect of Ground and/or Ceiling Planes on Thrust of Rotors in Hover

Vernon J. Rossow, Ames Research Center, Moffett Field, California

July 1985

National Aeronautics and
Space Administration

Ames Research Center
Moffett Field, California 94035

SUMMARY

The thrust produced by a helicopter rotor hovering near ground and/or ceiling planes is investigated experimentally and theoretically. In the experiment, the thrust was measured on a 0.324-m-diam rotor operating between floor and ceiling planes which were located from 6 to 0.08 diam from the rotor disk. In the first theoretical model studied, the incompressible and inviscid flow induced by a sequence of vortex cylinders, located above and below the rotor to simulate the rotor wake and its interaction with the floor and ceiling planes, was considered. Comparison with experiment showed that this model overpredicts the change in thrust caused by the proximity of the walls. Therefore, a second arrangement of vortex cylinders was introduced which provides a more accurate prediction of the ground and ceiling effects on the thrust of the rotor in hover. The applicability of these results to a vented wind tunnel is also discussed.

LIST OF SYMBOLS

AR_b	aspect ratio of rotor blade = r_b/c
c	chord of rotor blade, m
C_L	airfoil lift coefficient
C_T	rotor thrust coefficient = thrust/$\rho\pi\Omega^2 r_b^4$
D	rotor diameter = 2 r_b, m
$F(\mathscr{R})$	Bartky integration function
h	height of vortex cylinder, m
N_b	number of rotor blades
r_b	radius of rotor disk = D/2, m
r_v	radius of vortex ring or vortex cylinder, m
r,θ,z	cylindrical coordinate system; z perpendicular to rotor disk, m

$\mathcal{R}$	Bartky integration parameter
T	rotor thrust, N
T_σ	C_T/σ^2
u, v_θ, w	velocity components in radial, circumferential, and axial directions, m/sec
z_c	distance from rotor disk to ceiling plane, m
z_g	distance from ground plane to rotor disk, m
z_{im}	location of image vortex cylinder for ceiling plane, m
z_v	vertical location of vortex ring, m
α_b	geometric angle of attack on rotor blade, rad
α_e	effective angle of attack on rotor blade = $\alpha_b + \alpha_i$, rad
α_i	induced angle of attack on rotor blade = w/v_θ, rad
γ	circulation per unit length of vortex cylinder, m/sec
Γ	circulation bound in rotor blade, m^2/sec
σ	rotor solidity parameter, $N_b/\pi \mathcal{R}_b$
ψ	stream function, m^2/sec
Ω	rotor angular velocity, rad/sec

INTRODUCTION

There are substantial savings to be gained if a helicopter can be tested at velocities from those of hover up through maximum forward flight with a single setup in a wind tunnel. Unfortunately, at speeds near hover, an unknown portion of the energized wake of the rotor recirculates along the floor and walls of enclosed wind tunnels so that the wake interacts with other components of the vehicle and also reenters the rotor flow field. The complexity of the multienergy flow field of a rotor in the wind-tunnel test-section environment has not only delayed the solution of these flow fields, but also the development of guidelines for venting wind tunnel test sections to reduce such recirculation to a negligible level.

As a step toward understanding the flow field induced by a hovering rotor in a partially confined area, the present investigation was undertaken to study

experimentally and theoretically a simpler flow field, one that consists of a rotor in hover between large ground and ceiling planes. Such a configuration could be an approximation to a test wherein the sidewalls of the wind tunnel have been folded out of the way, leaving only the floor and ceiling surfaces near the rotor. Although the boundaries may still influence the test results, such an arrangement has some of the desirable characteristics of a vented wind tunnel, in that recirculation of the energized wake of the rotor is usually negligible. This attribute permits the analysis to be based on a steady-state assembly of vortices and vortex cylinders that represent the various flow-field components.

Previous theoretical estimates of the loads on rotor blades with and without a ground plane present have progressed from the quite simple and approximate model suggested by Betz (ref. 1) to relatively sophisticated and detailed simulations (e.g., refs. 2-11). The background research most relevant to this investigation are the two studies conducted by Knight and Hefner (refs. 2,3) in which the characteristics of vortex cylinders were used to calculate the loading and torque on rotors in free space (ref. 2) and in the presence of a ground plane (ref. 3). They also measured the thrust and torque on several rotors and compared the results with theory.

The research results presented here extend the previous work by considering the effect of both a ceiling and a ground plane on the thrust of a rotor in hover. An experimental program, described in the appendix of this paper, was carried out to obtain data with which the results of theoretical methods could be compared. The first theoretical method considered here is an extension of the one used by Knight and Hefner (refs. 2,3) in which vortex cylinders of constant diameter were used to simulate the wake of the rotor. In their analysis of ground effect (ref. 3) it was necessary to be quite approximate because a practical method for evaluating the integrals that describe the incompressible and inviscid flow field around vortex cylinders of finite length was not available at that time. The development (refs. 12,13) of a rapid and accurate method for numerically evaluating integrals of the elliptic type made it possible to carry out the analyses described in this paper. This numerical method removed limitations--imposed on Knight and Hefner--on the number of vortex cylinders that could be used in the flow field model and on the accuracy and ease with which the theoretical velocity components could be evaluated. Therefore, consideration can now be given to more detailed, complete, and consistent flow-field models for energized wakes in determining their attributes and failings.

The first model considered here simulates the rotor wake with a set of concentric vortex cylinders each of which extends from the rotor disk down to the ground plane. The presence of the ground and ceiling planes is simulated by placing a series of images above and below the tunnel region with the same set of concentric vortex cylinders used to represent the wake. When comparisons with the experiments are made of the thrust on a rotor in hover as predicted by a theory based on such an incompressible and inviscid wake model, it is found that the effect on downwash of the proximity of ground and ceiling planes is overemphasized. A semiempirical wake model is then introduced that provides usable and fairly accurate predictions of rotor thrust with both ground and ceiling planes nearby. The comparisons made here

are based on rotor thrust because it is sensitive to ground and ceiling plane proximity and because it could be measured accurately enough to test theoretical models.

VORTEX-CYLINDER SIMULATION OF ROTOR-WAKE FLOW FIELDS

The lift, drag, and torques acting on the blade elements that make up a rotor are a consequence of the rotary motion of the blade, and of the interaction of these vortex systems with nearby boundaries or walls. Since the vortex wakes are often unstable, the wake shape (idealized in fig. 1) becomes irregular and unsteady in character so that an exact solution would be quite complicated. It is assumed that a detailed knowledge of many of the local irregularities and oscillatory load variations is not needed for an understanding of tunnel-wall effects. The validity of this assumption will be verified by comparing theory and experiment. Therefore, the curved wake shown in figure 1 as a solid line is approximated by the right circular cylinder of constant diameter and constant strength, indicated by the double-dashed lines in figure 1. In most rotors, the blade loading is not ideal; as a result, circulation is shed not just at the blade tips but also all along the rotor radius. A proper representation of such a wake then requires not one but a continuous distribution of concentric vortex cylinders whose radii vary from the innermost lifting element out to the blade tip. This continuous distribution is approximated here by as few as 10 and as many as 80 concentric vortex cylinders.

When neither a ground nor ceiling plane is present, the vortex cylinders are semi-infinite in length, which gives them the characteristic of inducing at the rotor disk a constant downwash inside and a zero downwash outside the cylinder. This feature permits an easy solution for the blade loading when no boundaries are nearby, because the load on outboard blade elements is independent of inboard elements (refs. 2,3). If, however, the rotor is near a large surface, the velocity field induced by an image-vortex system couples the inboard and outboard blade segments because both inboard and outboard image-vortex cylinders then contribute to the downwash velocity at the rotor disk. A computation of the downwash field through the rotor disk then requires an iterative process between blade loading and wake structure.

The stream function ψ and the radial and axial velocity components are constructed from the incompressible and inviscid flow solutions for a vortex ring (ref. 14). Summation of a continuous distribution of vortex rings of constant diameter and strength along the length of the cylinder leads to the following double integrals

$$\psi = \frac{\gamma}{\pi}\int_0^h \int_0^{\pi/2} \frac{r r_v \cos 2\phi \, d\phi \, dz_v}{[(z - z_v)^2 + r^2 + r_v^2 - 2rr_v \cos 2\phi]^{1/2}} \tag{1a}$$

$$u = -\frac{\gamma}{\pi}\int_0^h \int_0^{\pi/2} \frac{r_v(z - z_v)\cos 2\phi \, d\phi \, dz_v}{[(z - z_v)^2 + r^2 + r_v^2 - 2rr_v \cos 2\phi]^{3/2}} \tag{1b}$$

$$w = \frac{\gamma}{\pi}\int_0^h \int_0^{\pi/2} \frac{r_v(r \cos 2\phi - r_v) d\phi \, dz_v}{[(z - z_v)^2 + r^2 + r_v^2 - 2rr_v \cos 2\phi]^{3/2}} \tag{1c}$$

where r_v is the radius of the rings and of the cylinder. The numerical effort is considerably reduced when the integration over z_v, the vertical location of the vortex ring element, is carried out analytically over the length of the cylinder. If this operation is followed by an integration by parts, the indeterminate form of the solutions at $r = 0$ is removed, and the integrals for a finite-length vortex cylinder may be written as

$$\psi = \frac{\gamma r_v}{\pi}\int_0^{\pi/2} r \cos 2\phi \, \ln\left[\frac{(z - h) + [(z - h)^2 + r^2 + r_v^2 - 2rr_v \cos 2\phi]^{1/2}}{z + [z^2 + r^2 + r_v^2 - 2rr_v \cos 2\phi]^{1/2}}\right] d\phi \tag{2a}$$

$$u = -\frac{\gamma}{\pi}\left\{\int_0^{\pi/2} \frac{r_v \cos 2\phi \, d\phi}{[(z - h)^2 + r^2 + r_v^2 - 2rr_v \cos 2\phi]^{1/2}} - \int_0^{\pi/2} \frac{r_v \cos 2\phi \, d\phi}{[z^2 + r^2 + r_v^2 - 2rr_v \cos 2\phi]^{1/2}}\right\} \tag{2b}$$

$$w = \frac{\gamma}{\pi}\int_0^{\pi/2} \frac{r_v(r \cos 2\phi - r_v)}{[r^2 + r_v^2 - 2rr_v \cos 2\phi]}\left\{\frac{z - h}{[(z - h)^2 + r^2 + r_v^2 - 2rr_v \cos 2\phi]^{1/2}} - \frac{z}{[z^2 + r^2 + r_v^2 - 2rr_v \cos 2\phi]^{1/2}}\right\} d\phi \tag{2c}$$

where the lower end of the cylinder is centered at $x = y = z = 0$. When the length of the cylinder h is increased indefinitely, the solutions for a semi-infinite vortex cylinder of uniform strength along its length becomes

$$\psi = \frac{\gamma}{\pi}\int_0^{\pi/2} rr_v \cos 2\phi \, \ln\left[z + \sqrt{z^2 + r^2 + r_v^2 - 2rr_v \cos 2\phi}\right] d\phi \tag{3a}$$

$$u = \frac{\gamma}{\pi}\int_0^{\pi/2} \frac{r_v \cos 2\phi \, d\phi}{[z^2 + r^2 + r_v^2 - 2rr_v \cos 2\phi]^{1/2}} \tag{3b}$$

$$w = \frac{\gamma}{\pi}\int_0^{\pi/2} \frac{r_v(r \cos 2\phi - r_v)}{[r^2 + r_v^2 - 2rr_v \cos 2\phi]} \left\{1 + \frac{z}{[z^2 + r^2 + r_v^2 - 2rr_v \cos 2\phi]^{1/2}}\right\} d\phi \tag{3c}$$

Along the axis of the vortex cylinder, the flow-field parameters may be written in closed form as

$$\psi = 0 \tag{4a}$$

$$u = 0 \tag{4b}$$

$$w = -\frac{\gamma}{2}\left\{\frac{z - h}{[(z - h)^2 + r_v^2]^{1/2}} - \frac{z}{[z^2 + r_v^2]^{1/2}}\right\} \tag{4c}$$

Evaluation of the integrals in equations (2) can be carried out accurately by using a modified form of Bartky's method (refs. 12,13). In order to apply the method, the integrals are first rewritten in terms of an integration parameter $\mathscr{R}$ and an integrand function, $F(\mathscr{R})$, so that the integral for the stream function, for example, becomes

$$\psi = \int_0^{\pi/2} F_\psi(\mathscr{R}) \frac{d\phi}{\mathscr{R}} \tag{5}$$

In the computations carried out here, the integration parameter that was used is

$$\mathscr{R} = [z^2 + r^2 + r_v^2 - 2rr_v \cos 2\phi]^{1/2} \tag{6a}$$

$$= \{[z^2 + (r - r_v)^2]\cos^2 \phi + 2rr_v \sin^2 \phi\}^{1/2} \tag{6b}$$

which leads to

$$\cos 2\phi = (z^2 + r^2 + r_v^2 - \mathscr{R}^2)/2rr_v$$

The integrand functions for the three flow-field parameters in equations (2) are then

$$F_{\psi}(\mathcal{R}) = \frac{\gamma}{\pi} r r_v \mathcal{R} \ell n \left[\frac{z - h + (\mathcal{R}^2 - 2zh + h^2)^{1/2}}{z + } \right] \tag{7a}$$

$$F_u(\mathcal{R}) = \frac{\gamma}{2\pi r} (z^2 + r^2 + r_v^2 - \mathcal{R}^2) \left[1 - \frac{\mathcal{R}}{(\mathcal{R}^2 - 2zh + h^2)^{1/2}} \right] \tag{7b}$$

$$F_w(\mathcal{R}) = \frac{\gamma(\mathcal{R}^2 + r_v^2 - r^2 - z^2)}{2\pi(\mathcal{R}^2 - z^2)} \left[z - \frac{\mathcal{R}(z - h)}{(\mathcal{R}^2 - 2zh + h^2)^{1/2}} \right] \tag{7c}$$

Since the choice of $\mathcal{R}$ is not unique, other forms of $\mathcal{R}$ and $F(\mathcal{R})$ could have been used to achieve the same numerical result. It should also be noted that the corresponding relationships for a vortex cylinder that is semi-infinite in length are derived from equations (3), or by finding the limiting forms of equations (7) as $h \to \infty$.

EXAMPLES OF STREAMLINE PATTERNS INDUCED BY VORTEX CYLINDERS

Before proceeding with the computation of the thrust on a rotor in hover, several streamline patterns are presented to illustrate the flow fields generated by vortex cylinders and their superposition. Since both the stream function ψ and the velocity components are easily calculable, both are used in a predictor/corrector type of calculation to find streamline paths that follow lines of constant stream function. The streamlines shown in figures 2-6 were started at equal radial increments across the vortex cylinder halfway along its length or where the cylinder crosses the edge of the figure.

The flow field induced by a semi-infinitely long vortex cylinder is presented in figure 2(a). Some of the streamlines are noted to cross the vortex surface. As is well known, the axial velocity at the open end of the cylinder is constant and equal to one half of its value inside the cylinder far downstream. Hence, half of the fluid enters the cylinder through the open end and half through the side wall. Such is not the case, however, for an actual vortex wake shed by a rotor, because all of the fluid in the wake enters through the rotor and stays inside the curved wake. Hence, in the idealized wake, with or without boundaries, no fluid crosses the vortex sheet because it curves to follow the streamline.

Figure 2(b) illustrates the flow field produced by superposition of two semi-infinite vortex cylinders facing each other across a ceiling plane. This configuration provides a model of a rotor wake and its induced streamlines when a ceiling plane is nearby. The image-vortex cylinder causes the downwash velocity across the cylinder opening to no longer be constant nor equal to half its value at great

distances from the opening. The change in downwash is, of course, representative of the change in thrust on the rotor as it approaches a ceiling plane.

Figure 3 presents the streamline patterns induced by vortex cylinders of two different lengths. In both cases, streamlines again cross the cylindrical vortex surfaces. Also, the axial velocity at the ends is not constant, even though other image cylinders are not present. The presence of a ground plane is simulated by placing a vortex cylinder of the same size but of opposite strength under the ground plane so that the ground plane becomes a streamline surface, as shown in figure 4. The rotor disk is assumed to be located at the top of the cylinder used to represent the wake. The streamlines in figure 4 indicate that all of the fluid in the flow field continually circulates through the rotor. The theoretical flow field outside the vortex cylinders is then probably not very representative of the flight situation, even though, as will be seen in the following sections, the downwash at the rotor appears to be simulated with some accuracy.

The presence of both a ceiling and a ground plane requires a series of images above and below the test section rather than a single image, as used in figures 2(b) and 4. In principle, an infinite series of images is needed to satisfy exactly the no-flow-through condition at both the ceiling and the floor. It was found, however, that a small number of images provides sufficient accuracy if the images are added to the original vortex system as a pair above and a pair below (see fig. 5). That is, the setup of the flow field is started with a wake vortex cylinder that extends from the rotor disk to the ground plane and with its image just below the ground plane. Thereafter, four image cylinders (two above and two below the test section) are added at once. Since these contributions are symmetrical about the ground plane, it remains a stream surface. The contributions to the velocity at the ceiling plane appear to decrease as fast as or faster than the square of the distance from the rotor disk. Hence, it was found that when three image systems (12 vortex cylinders) were added to the original wake cylinder and its image (14 vortex cylinders in all), the velocity components and the stream function were defined to about five significant figures.

Such a system of vortex cylinders was used to obtain the streamline pattern induced by one vortex cylinder located between a floor and ceiling, as shown in figure 6(a). Since only one vortex cylinder was used to represent the wake, the solution in figure 6(a) simulates a rotor that sheds vortices only at the blade tip. Representation of the more complicated wakes of actual rotors, which shed vorticity all along the blades, is accomplished by superposition of a number of concentric vortex cylinders, as indicated by the cross-sectional view in figure 6(b). In the interest of clarity, vortex cylinders were used at only four radial stations to represent the wake and to compute the streamlines. The downwash induced by a rotor wake, as used for the thrust calculations in the following sections, is based on vortex cylinders located at 10 to 80 radial stations. Each of these wake cylinders is accompanied by 13 image cylinders so that the flow field is based on a total of 140 or more vortex cylinders. The use of more image- or radial-vortex cylinders did not significantly change the computed results, but the use of fewer cylinders did cause changes on occasion.

CALCULATION OF ROTOR THRUST

The solutions described in the previous section for the flow field induced by vortex cylinders are now used to develop a method for predicting the thrust of rotors operating in the presence of ceiling and ground planes. The predicted results will then be compared in the next section with data taken in this study (see appendix) and with the data of Knight and Hefner (refs. 2,3). Since the blade loading and wake structure are directly dependent on one another, an iterative procedure is used to solve for both. The first step in the process is to calculate the loading when no boundaries are present by using the method introduced by Knight and Hefner (ref. 2). This blade-load distribution yields a first estimate for the strengths of the vortex cylinders used to represent the wake of the rotor (fig. 7) when it is operating in a confined region. These vortex strengths are then used in equations (1)-(7) to calculate the downwash or upwash induced by a series of concentric, shortened (rather than infinite-in-length) vortex cylinders that represent the shed vorticity of the blade elements and the images in the ceiling and floor. From the new downwash distribution predicted by the system of vortex cylinders, a revised blade loading is calculated which in turn yields a new wake-vortex distribution for use in the downwash calculation. The cyclical process is continued until the change in wake structure and rotor thrust between computation cycles is negligible.

The following equations are used to relate the various flow-field parameters to the rotor configuration. The thrust or lift increment on a radial segment of a blade, c dr, is given by

$$dT = C_L \left(\frac{1}{2} \rho v_\theta^2\right) c \, dr = \rho \Gamma(r) v_\theta \, dr \tag{8a}$$

so that the bound circulation on a blade at the radius r is given by

$$\Gamma(r) = \frac{1}{2} C_L v_\theta c \tag{8b}$$

The circumferential velocity v_θ of the blade element relative to the air at that radius is given by

$$v_\theta = \Omega r - N_b \Gamma(r)/4\pi r \tag{9}$$

where Ω is the rotor angular velocity and N_b is the number of rotor blades in the rotor. The contributions to v_θ and to other parameters by the images in the ceiling and floor of the bound circulation in the blades is assumed negligible in this analysis. In fact, the effect of the second term in equation (9), which represents the effect of the circulation shed along the rotor axis, is usually small. The lift coefficient C_L on a blade element is dependent on the geometric blade angle α_b, and the induced angle α_i, because of the downwash,

$$\alpha_i = \tan^{-1} w/v_\theta \approx w/v_\theta \tag{10}$$

which combine to give the effective angle of attack α_e, as

$$\alpha_e = \alpha_b + \alpha_i \approx \alpha_b + w/v_\theta \tag{11}$$

where w is taken as positive when upwash occurs. The lift coefficient C_L is based on two-dimensional theory or data at the effective angle of attack α_e for the element as given by equation (11). It was found convenient here to approximate the two-dimensional experimental data (e.g., those of refs. 2 and 15) on the airfoils taken at the test Reynolds numbers with four terms of the power series equation,

$$C_L = \alpha_e C_{L1} + \alpha_e^2 C_{L2} + \alpha_e^3 C_{L3} + \alpha_e^4 C_{L4} \tag{12}$$

The wake-induced vertical velocity w through the rotor disk is found as a sum of the velocities induced at the radius r by all of the vortex cylinders (figs. 6,7). The strength or circulation per unit length γ of the wake-vortex cylinder at the radius $r = r_v$, is related to the change with radius of the bound circulation $\Gamma(r)$ on the blade, and the downwash velocity w, at the radius of the vortex cylinder. The criterion chosen here to relate the shed vorticity and the downwash velocity is an extension of the one used for a rotor operating in an unbounded region. That is, if no boundaries are present, the vortex cylinder is semi-infinite in length so that the velocity induced at the rotor disk is one half that inside the cylinder far below the rotor:

$$w_{\substack{z=0 \\ r<r_v}} = \frac{1}{2} \cdot w_{\substack{z=-\infty \\ r<r_v}}$$

Based on the characteristics of semi-infinite vortex cylinders, the vertical velocity just outside the cylinder vanishes:

$$w_{\substack{r=r_v^+ \\ z=-\infty}} = 0$$

The circulation per unit length of the vortex cylinder yields the best values of thrust if it is related to the shear across the vortex layer at infinity (and not at the rotor disk) by

$$\gamma = \text{circulation/unit length} = (w_{inside} - w_{outside})_{z=-\infty} \tag{13a}$$

where w_{inside} and $w_{outside}$ are the vertical velocity components just inside and just outside the vortex cylinder being considered. When the vortex cylinder that represents the wake extends to $z = -\infty$, the downwash velocity induced at the rotor disk is half that at infinity. The circulation per unit length of the cylinder is given by

$$\gamma = 2 \cdot (w_{inside} - w_{outside})_{z=0} \tag{13b}$$

The idealized rotor wake depicted in figure 1 extends to infinity in a radial rather than a vertical direction. In both cases, the velocity vanishes outside the wake far from the rotor. Equation (13b) instead of equation (13a) is used to relate the circulation in the vortex cylinder to the downwash distribution in the general case when both ground and ceiling planes are nearby. Once γ is known, equations (1)-(4) are used to calculate the downwash velocities induced by the vortex cylinders. This computation is made by relating the vorticity shed by the rotor blades on each revolution to the downwash velocities to obtain another relationship for γ. The change in the circulation bound in a rotor blade, $\Delta\Gamma(r)$, over a radial increment Δr, can then in the general case again be related to the downwash velocity at the rotor disk by

$$\gamma = \Delta\Gamma(r)/\Delta z$$

where Δz is the vertical spacing between the vortices shed by the rotor blades and given by

$$\Delta z = \frac{2\pi}{\Omega N_b} \cdot w_{ave}$$

and

$$w_{ave} = \frac{1}{2}\left(w_{inside} + w_{outside}\right)_{z=-\infty}$$

$$= \left(w_{inside} + w_{outside}\right)_{z=0}$$

In the computer code for the thrust, the vortex cylinders and the other parameters used in the computations were set up in arrays. Since the vertical velocity, w_{inside}, on the inside surface of a vortex cylinder is then also the vertical velocity on the outside of the next inboard cylinder, $w_{outside}$, a single vertical velocity w, suffices for both, because its location relative to each vortex cylinder determines whether it is used as an inside or an outside velocity.

As mentioned previously, the iterative process in the computations is begun by evaluating, for example, the downwash distribution, the strength of the vortex cylinders, and the thrust when the rotor is operating in an unbounded region. Under those circumstances, the downwash through the rotor may be written as (assuming a linear lift curve and that $v_\theta = \Omega r$)

$$w = \Omega N_b\left[cC_{L1} - \left(c^2C_{L1}^2 + 16\pi cC_{L1}\alpha_b r/N_b\right)^{1/2}\right]/8\pi \qquad (14)$$

where the negative sign was chosen on the square root to insure that the velocity w is negative so that downwash rather than upwash is predicted. From the radial distribution of w predicted by equation (14) for the rotor in an unbounded space, a first estimate for the circulation bound to the blades and shed into the wake is determined. The iterative procedure described previously is then used to refine the calculations for the flow-field structure and the thrust. Throughout the analysis, the radial velocity u_r induced by the wake-vortex cylinders, is assumed to have a negligible effect on the loading.

COMPARISON OF PREDICTED AND MEASURED ROTOR THRUST

Experimental Data Used for Comparisons

The thrust predicted by two wake models is now compared with two sets of experimental data. One set of data was taken by Knight and Hefner (refs. 2,3) with a rotor at various distances from a ground plane and presumably with no overhead or side boundaries. Their rotor was 1.524 m in diameter and could be tested with two to four untwisted blades that had NACA 0015 airfoil sections with chords of 5.08 cm and angles of attack from 0° to 14°. The maximum Reynolds Number at the blade tips was about 250,000. The diameter of the circular ground plane was 2.5 times the diameter of the rotor (3.66 m) and could be located at distances from 0.125 to 1.1 rotor diameters below the rotor disk.

Since a systematic set of thrust measurements on a rotor operating in both ground and ceiling effect was not available, the first part of this investigation was devoted to the experiment described in the appendix. The rotor (ref. 16) used was 0.324 m in diameter and had two untwisted blades with chords of 2.65 cm. The maximum test Reynolds number at the blade tips was 167,000. The airfoil section tapered from a NACA 0020 section at the 0.235 r_b radius where the blade became a rectangular nonlifting section to a NACA 0008 section at the tip. The blades were set at a geometric angle of attack of $\alpha_b = 11.6° \pm 0.1°$ for the entire test, and the ground plane was from 0.08 to 1.92 rotor diameters and the ceiling plane at distances from 6 to 0.08 rotor diameters from the rotor disk. The appendix of this paper describes the equipment and procedures used to conduct the test.

The most noteworthy characteristic of the data obtained in the experiment conducted for this investigation is that the thrust varied nearly linearly with the logarithm of the distance of the rotor disk from the ground or ceiling plane as shown by the lines in figure 8 made up of long dashes. This characteristic appears to be valid whether the ceiling or ground plane is held fixed while the other plane is moved inward or outward. The total scatter in the thrust data is indicated by bars on the end of a vertical line for the fixed ground plane data and by a rectangular box for the fixed ceiling data. In both cases the mean value of all of the data taken at each configuration is indicated by a dot.

Thrust Predicted by Wake Model Based on Complete Image System

The theoretical model described previously was used to predict the thrust values shown in figure 8 by the short-dash lines. As mentioned in the description of the theory, the wake model used 14 vortex cylinders at 10 to 80 radial stations that were arranged so that the ceiling and ground planes were streamline surfaces. The computations were begun by calculating the thrust on the rotor in unconfined space and then moving the ground plane up to 1.92 diam below the rotor disk. Values used for the dashed curve labeled $z_c/D = 6.0$ were generated by leaving the ceiling far from the rotor but continual stepwise movement of the ground plane nearer the rotor produced the curve shown. The dashed curve labeled $z_g/D = 1.92$ was produced

by leaving the ground plane at its maximum distance of 1.92 diam below the disk (as occurs in the experiment) and moving the ceiling plane stepwise toward the rotor. Both curves are noted to have the same character exhibited by the experimental data; namely, the approximate linear change of thrust with the logarithm of the distance of the rotor to the ceiling or ground. However, both theoretical curves lie substantially above the experimental data.

Since the Reynolds number and scale of the present test were small, various attempts were made to find lift-curve equations that would bring the theory more in line with the experiment. It was found that the curves could be lowered by this technique so that a portion of the theoretical curves was close to the experimental data at values of z_g/D and z_c/D that were less than about 0.5. However, the thrust for larger distances was then underpredicted. It was concluded, therefore, that strict adherence to the complete wake-vortex image system will overestimate the downwash and thrust changes caused by ground and ceiling plane proximity. Such a conclusion is supported by the observation that the shape of the idealized rotor wake as it impinges on the ground plane is bell shaped, whereas the theoretical wake consists of cylinders of constant radius. This difference in shape causes the theoretical images to maintain a columnated or focused upwash onto the rotor disk; the more realistic bell-shaped image vortex system (fig. 1) would tend to disperse the upwash. Hence, the use of vortex cylinders for the simulation of wake elements is convenient and straightforward, but such a model appears to overpredict the effects of ceiling and ground planes on upwash.

Thrust Predicted by Wake Model Based on Two Vortex Cylinders

The comparisons made of the theory based on the complete image system with the data taken on the small 0.324-m rotor indicate that the theory correctly represents the nature of the thrust change but not the magnitude of the change caused by the proximity of the floor and ceiling planes. Attempts were made, therefore, to find a wake and image system with vortex cylinders that would correctly predict the level of the thrust. It was first noted that as the rotor approaches the ground plane, the calculated downwash velocity through the rotor decreases, both because the vortex cylinder that represents the wake shortens (and therefore contains less circulation) and because the image-vortex cylinder immediately under the ground plane gets nearer the rotor. One way to reduce the effect of ground proximity on downwash is to eliminate the image cylinder immediately below the ground plane. It was found that this simplified model of the wake with the ground plane is a good approximation; the thrust predicted on the small (0.324-m diam) rotor as it approaches the ground plane is shown by the upper solid line in figure 8. The agreement is excellent, even though such a model violates the no-flow-through condition at the ground plane.

A representation of the effect of the ceiling on thrust similar to the one for ground effect was neither so easy nor accurate. It was reasoned that an image-vortex cylinder identical with the one used to represent the wake is needed above the ceiling plane so that the rotor downwash is constrained as the rotor approaches

the ceiling. Not obvious was the location of the image cylinder above the ceiling relative to the rotor position; that is, $z_{im} = f(z_c)$, as indicated in figure 9. After a number of schemes were tried, the one chosen for the comparisons made here used the relationship

$$z_{im} = 5z_c^{1.25}$$

Hence, the curves shown as solid lines in figures 8, 10, and 11 were calculated with a wake model composed of concentric vortex cylinders between the rotor disk and the ground plane to represent the wake, and an identical image-set above the ceiling plane (see fig. 9).

It should first be noted that the predictions provided by the approximate wake system agree with the experiment much better than the results from the complete image system when only one plane--either ground or ceiling--is near the rotor. The predicted variation of thrust when both planes are present is illustrated in figure 10. Comparison of the theory with the data generated in the present study (see Appendix) for both ceiling and ground planes nearby is shown in figure 11. Generally good agreement is noted throughout. It is noted, however, that the theoretical result for the ceiling alone shown in figure 8 deviates considerably more from a straight line than the experimental data. Another semiempirical scheme that fits the data better could probably have been found, but other shortcomings in the theory suggest that effort spent on a completely new approach would probably be more advisable.

Comparison with the data of Knight and Hefner (refs. 2,3) provides a test of only the ground-plane simulation. Examination of the data for the two-dimensional flow around a NACA 0015 airfoil (refs. 2,15) at the Reynolds number of the test (Re ≈ 250,000) suggested a lift-curve equation as a function of effective angle of attack; the equation is given in the captions of figures 12 and 13. The lift equation was first tested on the data taken when the rotor was not confined by nearby boundaries (i.e., no ground plane), and minor adjustments were made in the coefficients to obtain the match presented in figure 12. The presence of the ground plane is noted in figure 13, again to be simulated quite accurately by the single image set of wake-vortex cylinders used in the approximate theory.

APPLICABILITY OF RESULTS TO VENTED WIND TUNNELS

One purpose of this investigation was to obtain theoretical and experimental information about rotors operating in confined regions; this information was needed for the development of guidelines for the design of vented wind tunnels. The objective of the vented wind-tunnel design is to achieve the capability to test helicopters or V/STOL aircraft at speeds from hover to maximum forward flight velocity. One approach to tunnel design is to have accommodating walls that conform to the streamlines that would occur around the vehicle if it were in free space. The

accommodation is accomplished either by curving the wall shape or by withdrawing and introducing air through porous walls to simulate curved walls.

In a second approach, the tunnel test section is designed to eliminate only those wall-interference contributions for which a correction owing to confinement is not possible. One such interference is the recirculation of the rotor wake or of the lifting jet exhaust back into the rotor or jet intake. Such a recirculation appears to be reduced to a negligible level if the side walls of the tunnel are open or far from the test vehicle, as assumed in the investigation reported here. One way to implement such a wind-tunnel configuration is to have the side walls of the tunnel made up of rotating louvers or hinged doors so that they can be opened for hover and for low-speed tests and closed for high-speed tests. It would seem that opening up the entire side wall of the test section is to be preferred over a partial opening of the side walls with doors near the floor and ceiling. Not only would a partial opening have to be tailored to the test device, but the necessary corrections would be much more difficult to derive for the general case.

When the configuration of the vented test section has been determined, it will be desirable to place the rotor at the location between the ceiling and ground planes that yields the minimum interference from the combined effects of those planes. This optimum height was calculated for a rotor in tunnels of different sizes, using the theory presented in this paper for both the 0.324-m and the 1.524-m rotors with two to five blades at geometric blade angles from 4° to 12°. All of the data fell near the curve shown as a solid line in figure 14. It is to be noted that when the rotor is large relative to the tunnel (i.e., $z_t/D \approx 0.4$), the rotor should be located at a point that is about 60% of the distance between the ground and ceiling planes, measured from the ground plane. When $z_t/D > 1$, the optimum location increases to about 73%. Also shown in figure 14 is a vertically hatched curve for the predicted range of thrust change caused by interference at the optimum location. Since an off-optimum location usually causes no more than a 4% additional thrust increment, a location near $z_g/z_t = 0.6$ is probably to be preferred if only one strut height is to be used.

As it applies to the wind tunnel venting system, the investigation reported here should be extended to determine the floor and ceiling areas needed outside the tunnel to prevent excessive recirculation of energized wakes. In addition, corrections have to be developed for the floor and ceiling proximity as the forward velocity increases from hover up to the velocity where the tunnel side doors can be closed. A more sophisticated wake model should probably be used in such an investigation, because the wake-vortex cylinders used here become unrealistic for simulation of the wake shape and the recirculation of the flow about a rotor.

CONCLUDING REMARKS

The experimental and theoretical investigation reported here provides information on the effect of ground and ceiling planes of the thrust of rotors in hover.

Of particular significance was the finding that the thrust change caused by surface proximity varied approximately linearly with the logarithm of the distance of the ceiling or ground plane from the rotor disk.

The theoretical part of the investigation reported here extends the theory of Knight and Hefner for a rotor in hover to include both a ground and ceiling effect by using an array of concentric vortex cylinders to simulate the wake of the rotor and its images above and below the tunnel test section. It was found that the theory properly represents the trend in thrust with surface proximity, but that it overpredicts the magnitude of the thrust change. A semiempirical modification of this basic method was then used to formulate a wake-cylinder model for the downwash; the wake-cylinder model consisted of a set of wake-vortex cylinders that extends from the rotor disk to the ground plane to represent the wake in ground effect. A single set of image-vortex cylinders is used to represent the ceiling effect. An equation for the location of the image-set of cylinders above the ceiling was adjusted to bring the predicted thrust in agreement with the measured thrust. This semiempirical model for the downwash induced by a rotor wake in hover predicts the thrust on the rotor tested here and on the ones tested by Knight and Hefner quite accurately at all of the ground-plane distances when the ceiling plane is not too near. The loss of some accuracy when both ground and ceiling planes are near the rotor is probably caused by breakdown of the flow field in the narrow space between the two planes.

Extension of the investigation to rotors moving at low forward speeds will necessitate the accumulation of data on a variety of confinement configurations and the development of an improved model for the rotor wake in the presence of confining walls. It may then be possible to apply the researcgh results to the design of vented wind tunnels that are capable of testing rotorcraft from hover speeds to maximum foward speeds.

APPENDIX

EXPERIMENTAL STUDY OF 0.324-m ROTOR IN GROUND AND CEILING EFFECT

A description is presented here of the experimental setup and procedures used to study the effect of ground or ceiling planes or both on the thrust of rotors durin$_{t}$ hover.

The two-bladed rotor used in the test is the same one used by Empey and Ormiston (ref. 16). The rotor is 0.324 m (12.75 in.) in diameter with two untwisted aluminum blades; the blade chord is 2.65 cm (c = 1.043 in.), and it blends into a nonlifting rectangular cross section at about 3.81 cm (1.5 in.) or $r/r_b = 0.235$. The airfoil thickness tapers from a NACA 0020 section at the inboard radius where the blade section becomes rectangular to a NACA 0008 at the tip. The geometric angle of attack of the blades is adjusted by first loosening clamping bolts at the hub, aligning the blades with a set of templates, and then tightening the bolts. The geometric angle of attack used in these tests was measured at $\alpha_b = 11.6° \pm 0.1°$.

The rotor shaft was mounted horizontally through a tube to help stabilize it against vibration. The end of the shaft opposite the rotor was attached to a variable-speed electric motor capable of speeds up to about 6,000 rpm. The entire assembly was suspended on two thin, flexible pieces of sheet metal and then restrained from horizontal motion by a 4.4N (1-lb) balance, as illustrated in figure 15. The rpm was detected by a magnetic pickup on the shaft and fed electronically into an analog-to-digital converter minicomputer system, along with the thrust force and atmospheric pressure and temperature; in this way, the thrust coefficient C_T was calculated automatically. The average of 15 readings of C_T was printed out five times at each experimental test condition. Data were taken at nominal rpm settings of 3,000 to 5,500 rpm at increments of 500 rpm. As noted in the text, the maximum and minimum of all of the values of C_T taken during the run sequence are shown as short horizontal bars at the end of a vertical line; the arithmetic mean of all the readings is indicated by a dot.

The floor and ceiling planes were made of plywood sheets standing on end, as shown in figure 15. Floor and ceiling sizes of 4 × 8 and 8 × 8 rotor diameters were used to be sure that both the ceiling and ground planes in the test were large enough to approximate an infinite size. Comparison of the measured thrust for the large surfaces with data for the small surfaces showed no systematic differences. It was concluded, therefore, that either size was adequate to approximate the infinite size assumed in the theory.

The rotor axis was about 5 diam above the floor of the test area and the whole assembly was located in a room about 30 diam on a side. The room was kept free of forced circulations from such sources as heaters, open doors, and windows during the data-taking process. Even though these precautions were taken, the thrust still varied over time periods of several seconds to several minutes. The total excursions of the thrust and the averaged values were repeatable on a given day or from

week to week. It is believed that the variations in thrust were due to unsteadiness in the wake and in the ingested flow, because time-dependent flow variations were observed in the energized wake as it passed the edges of the floor plane.

The test was conducted in approximately 1-hr increments, which were begun by reading the atmospheric pressure and temperature at the test site. A given ground-plane distance was chosen (i.e., between 1.92 D and 0.078 D) and the ceiling plane was removed from the test area. Data were taken as indicated previously at rpm values from about 3,000 to about 5,500 rpm in 500-rpm increments. The electric motor that drove the rotor was then turned off and the ceiling plane moved to a new desired distance. After the data-taking process was again completed, the ceiling plane was moved nearer the rotor disk and the process repeated. This procedure was continued until data had been obtained throughout a matrix of ground and ceiling distances which included z_g = 1.92 D to 0.0784 D and z_c = 6.0 D to 0.0784 D.

The thrust on the rotor in unconfined space as a function of geometric blade angle α_b, was obtained by Empey (e.g., ref. 16), and is presented in figure 16 to illustrate its variation and to provide a comparison with theory. The data taken at $\alpha_b = 11.6°$ in this test lie slightly below the data curve measured by Empey, probably because the blades are rougher than they were when tested by Empey (ref. 16). A theoretical curve for the thrust as a function of blade angle is also shown in figure 16. The thrust calculations require a lift-curve equation for the blade sections. Since the maximum Reynolds (based on blade chord) for the test was 167,000, the first lift-curve equation was an approximation to the data presented in reference 15 for Re = 42,000, 84,000, and 169,000. The coefficients of α_e in the equation were then adjusted slightly so that the computed thrust coefficients fit the unconfined data at $\alpha_e = 11.6°$, thereby resulting in the equation

$$C_L = 0.08\alpha_e - 0.00006\alpha_e^3 \qquad \text{(A1)}$$

Other lift-curve equations could have been used with approximately the same result, but equation (A1) provided satisfactory results throughout the range of experimental conditions.

REFERENCES

1. Betz, A.: The Ground Effect on Lifting Propellers. NACA TM-836, 1937 (see also Zeitschrift fuer angewandte Mathematik und Mechanik, 17, (2), Apr. 1937, pp. 68-72).

2. Knight, M.; and Hefner, R. A.: Static Thrust of the Lifting Airscrew. NACA TN-626, 1937.

3. Knight, M.; and Hefner, R. A.: Analysis of Ground Effect on the Lifting Airscrew. NACA TN-835, 1941.

4. Heyson, H. H.: Linearized Theory of Wind-Tunnel Jet-Boundary Corrections and Ground Effect for VTOL-STOL Aircraft. NASA TR R-124, 1962.

5. Hackett, J. E.; Wilsden, D. J.; and Lilley, D. E.: Estimation of Tunnel Blockage from Wall Pressure Signatures: A Review and Data Correlation. NASA CR-15,224, 1979.

6. DuWaldt, F. A.: Wakes of Lifting Propellers (Rotors) in Ground Effect. CAL No. BB-1665-S-3, 1966.

7. Landgrebe, A. J.: The Wake Geometry of a Hovering Helicopter Rotor and Its Influence on Rotor Performance. J. of the Am. Helicopter Soc. 17, (4), Oct. 1972.

8. Kocurek, J. D.; and Tangler, James L.: A Prescribed Wake Lifting Surface Hover Performance Analysis. J. of the Am. Helicopter Soc. 22, (1), Jan. 1977.

9. Johnson, W.: Comparison of Calculated and Measured Model Rotor Loading and Wake Geometry. NASA TM-81189, 1980.

10. Shenoy, K. R.; and Gray, R. B.: Iterative Lifting Surface Method for Thick Bladed Hovering Helicopter Rotors. AIAA J. of Aircraft, 18, (6), June 1981.

11. Miller, R. H.: Rotor Hovering Performance Prediction Using the Method of Fast Free Wake Analysis. AIAA Paper 82-0094, Jan. 1982.

12. Bartky, W.: Numerical Calculation of a Generalized Complete Elliptic Integral. Reviews of Modern Physics, 10, Oct. 1938.

13. Rossow, V. J.: On Bartky's Method for Evaluation of Integrals of Elliptic Type with Application to Round-Nosed Wedges. SIAM J. on Scientific and Statistical Computing, vol. 6, no. 2, April 1985, pp. 365-375.

14. Lamb, Sir Horace: Hydrodynamics, Dover Publications, 1945.

15. Jacobs, E. N.; and Sherman, A.: Airfoil Section Characteristics as Affected by Variations of the Reynolds Number. NACA TR-586, 1937.

16. Empey, R. W.; and Ormiston, R. A.: Tail-Rotor Thrust on a 5.5-Foot Helicopter Model in Ground Effect. Preprint No. 802, Presented at the 30th Annual National Forum of the American Helicopter Society, May 1974.

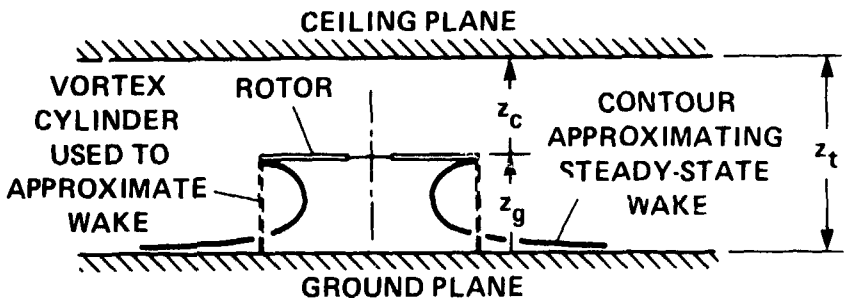

Figure 1.- Cross section of axially symmetric wake shapes used to approximate energized wake of rotors in presence of ground and ceiling planes.

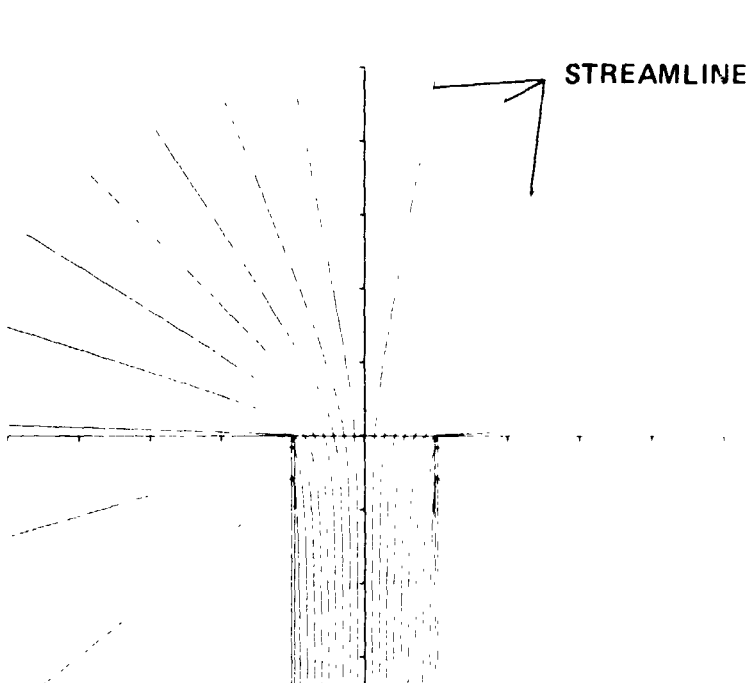

(a) No nearby boundaries.

Figure 2.- Streamlines of axially symmetric flow field induced by a semi-infinitely long vortex cylinder.

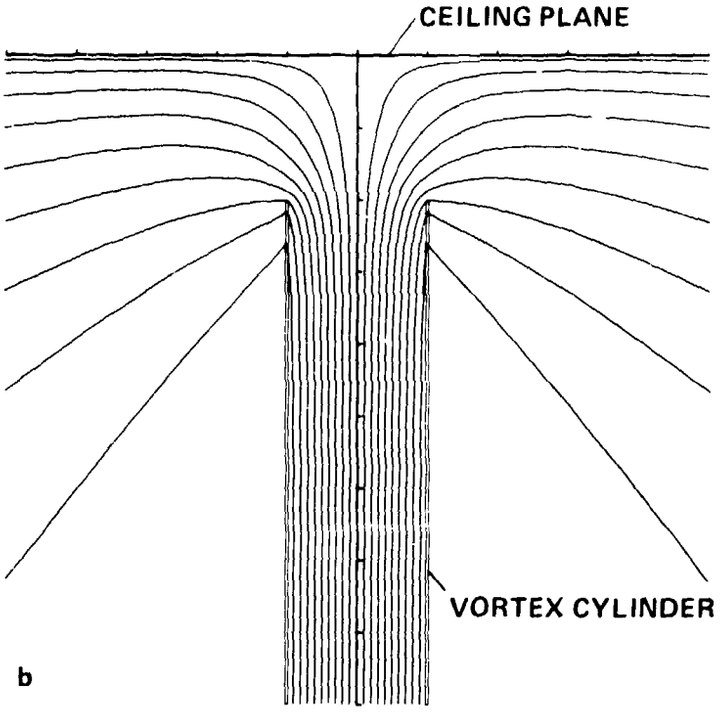

(b) With ceiling planes.

Figure 2.- Concluded.

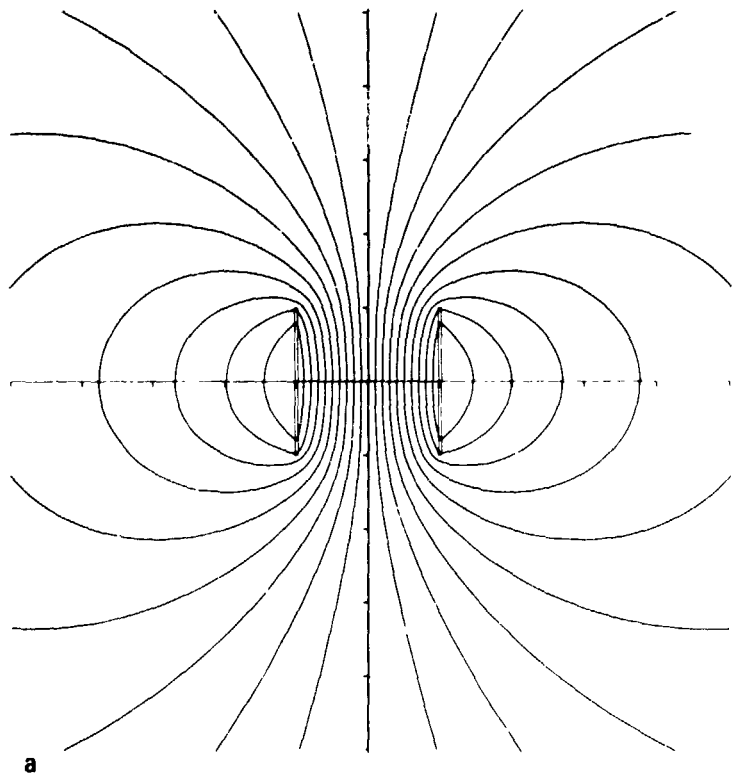

(a) $h = 2r_v$.

Figure 3.- Streamlines of axially symmetric flow field induced by vortex cylinders of finite length.

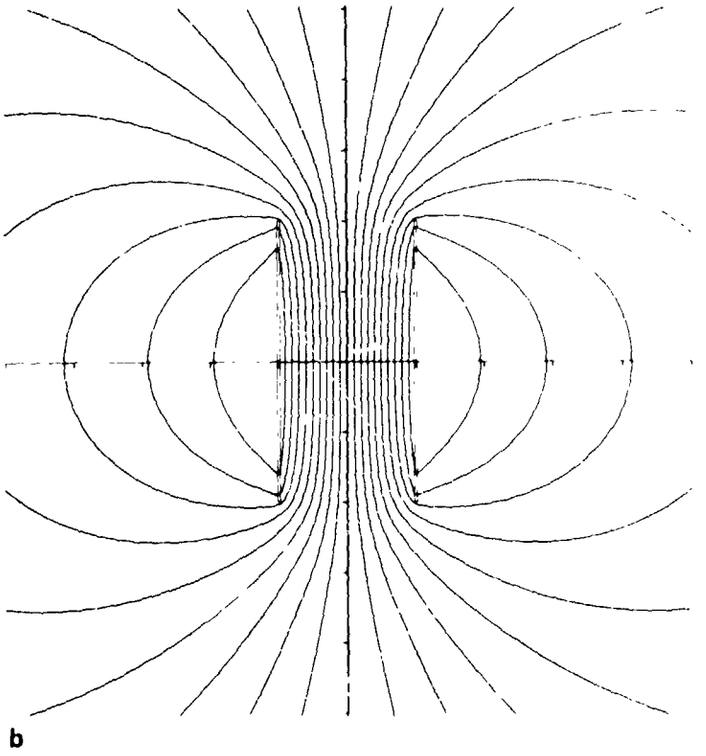

(b) $h = 4r_v$.

Figure 3.- Concluded.

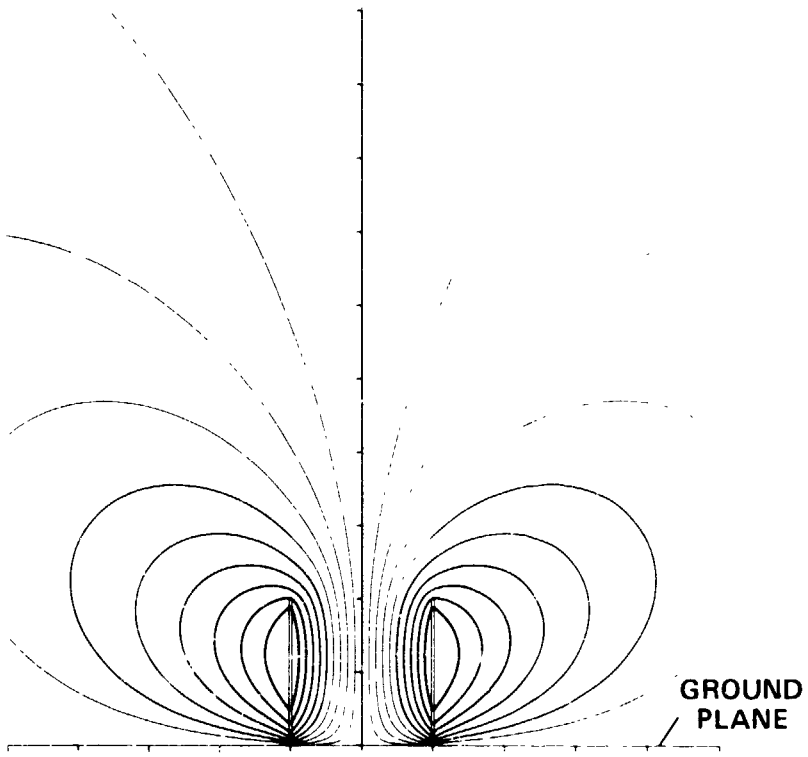

Figure 4.- Streamline pattern of axially symmetric flow field induced by vortex cylinder whose length is equal to its diameter: $h = 2r_v$, with ground plane present.

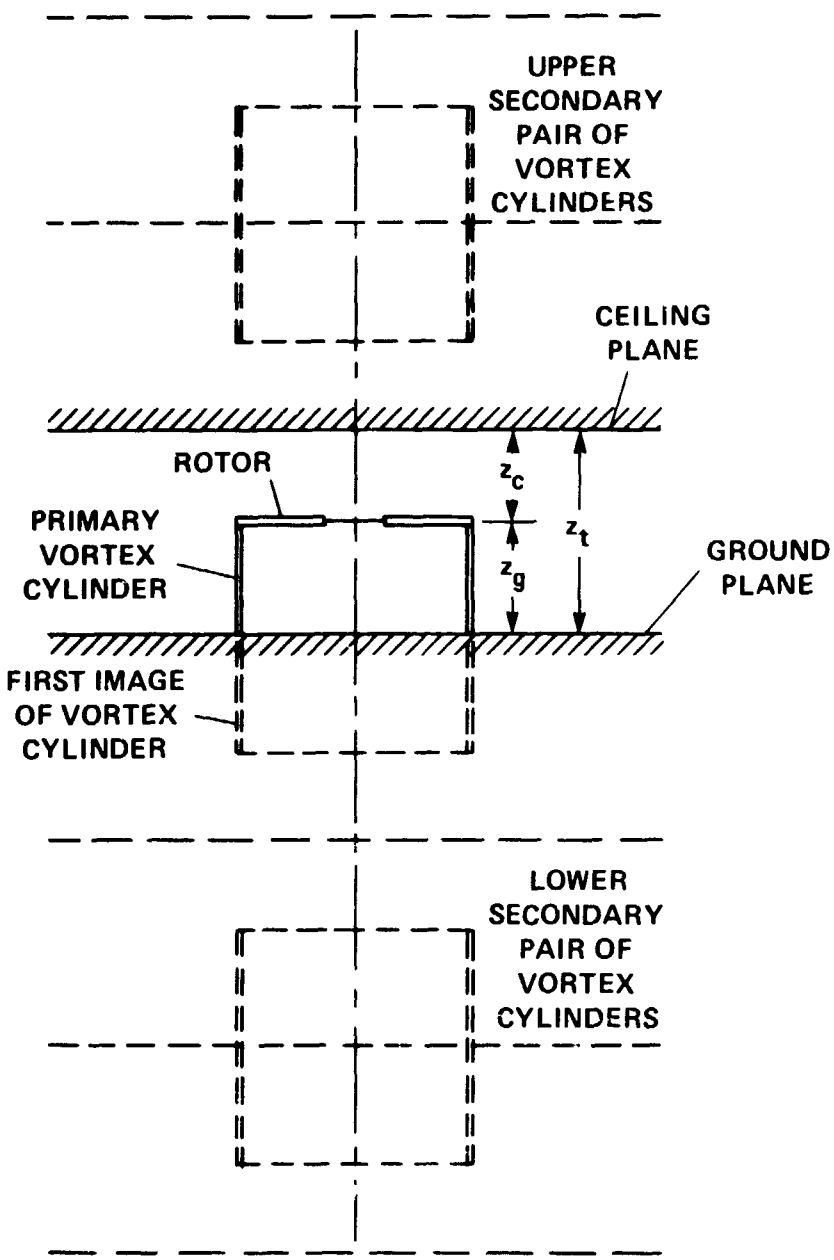

Figure 5.- Sketch of first part of imaging system used to simulate presence of both ground and ceiling planes on rotor flow field.

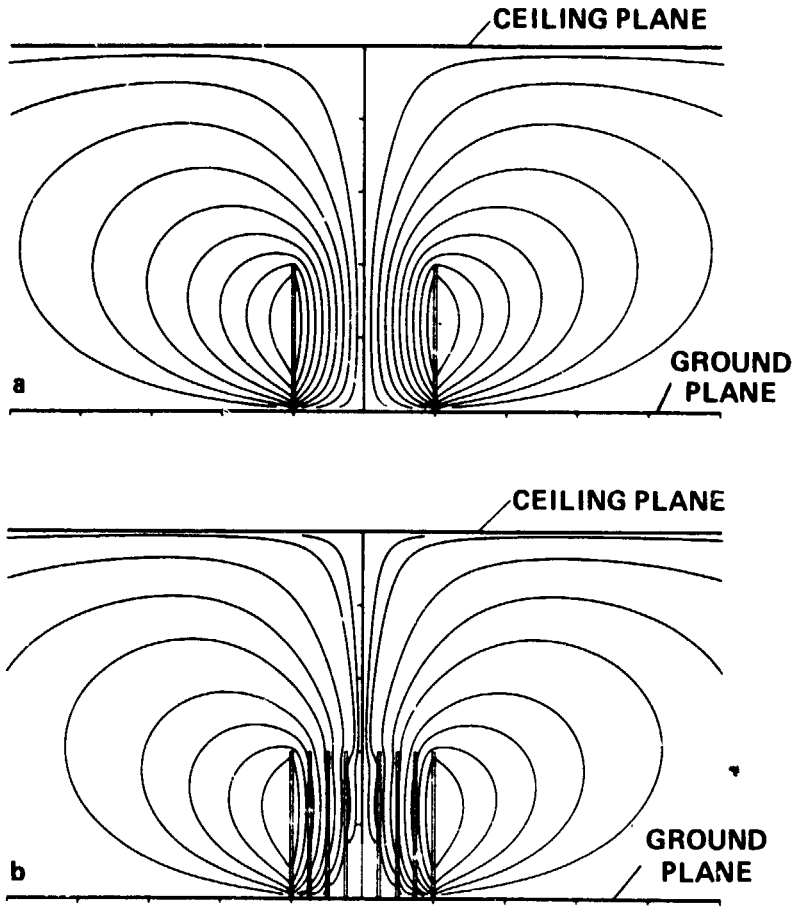

Figure 6.- Streamline pattern of axially symmetric flow fields induced by vortex wakes when ground and ceiling planes are present: (a) One vortex wake; (b) four vortex wakes; relative strengths of cylinders per unit length were determined by theoretical load on two-bladed rotor: $\gamma_1 = -1.00$, $\gamma_2 = +0.17$, $\gamma_3 = +0.20$, $\gamma_4 = +0.25$.

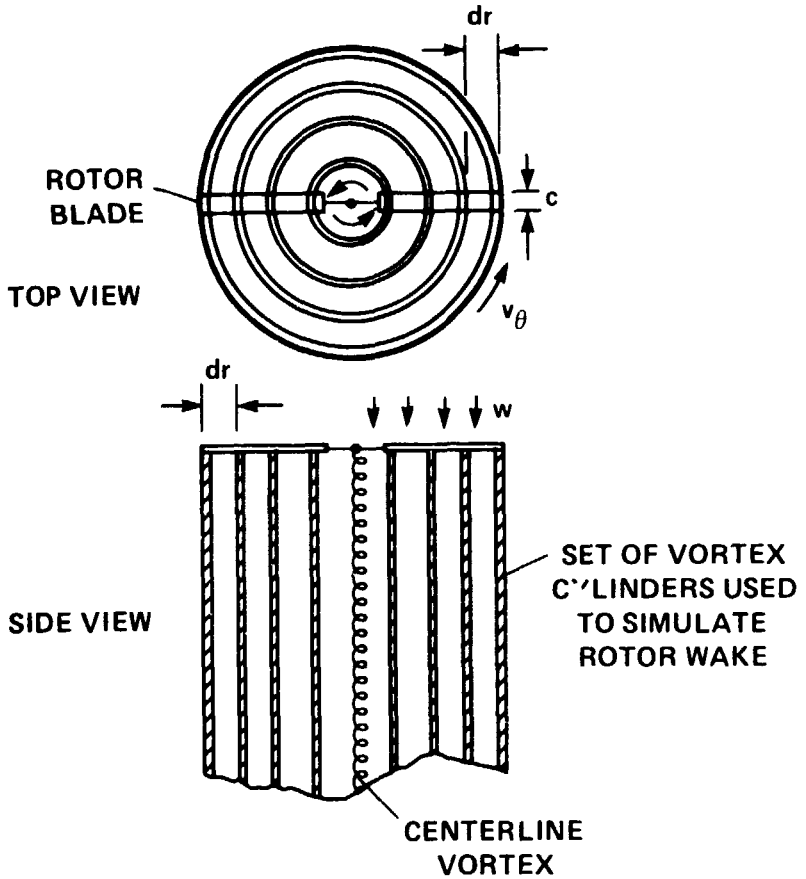

Figure 7.- Schematic of arrangement of vortex cylinders, rotor blades, etc., used in theory for predicting thrust.

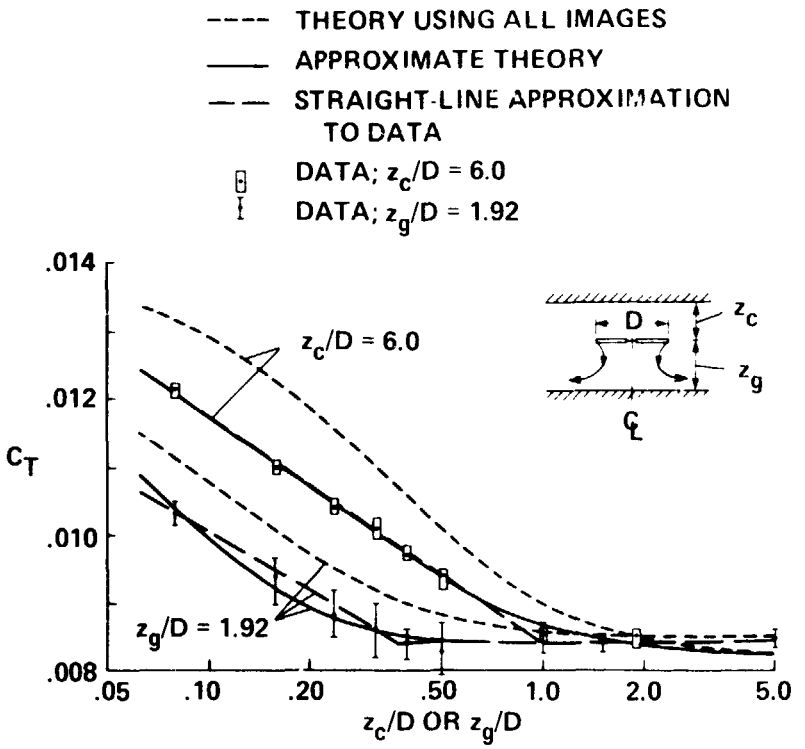

Figure 8.- Comparison of various theories with experiment on 0.324-m-diam (12.75-in.-diam) rotor: $C_L = 0.08\alpha_e - 0.00006\alpha_b^3$ $\alpha_b = 11.6° \pm 0.1°$.

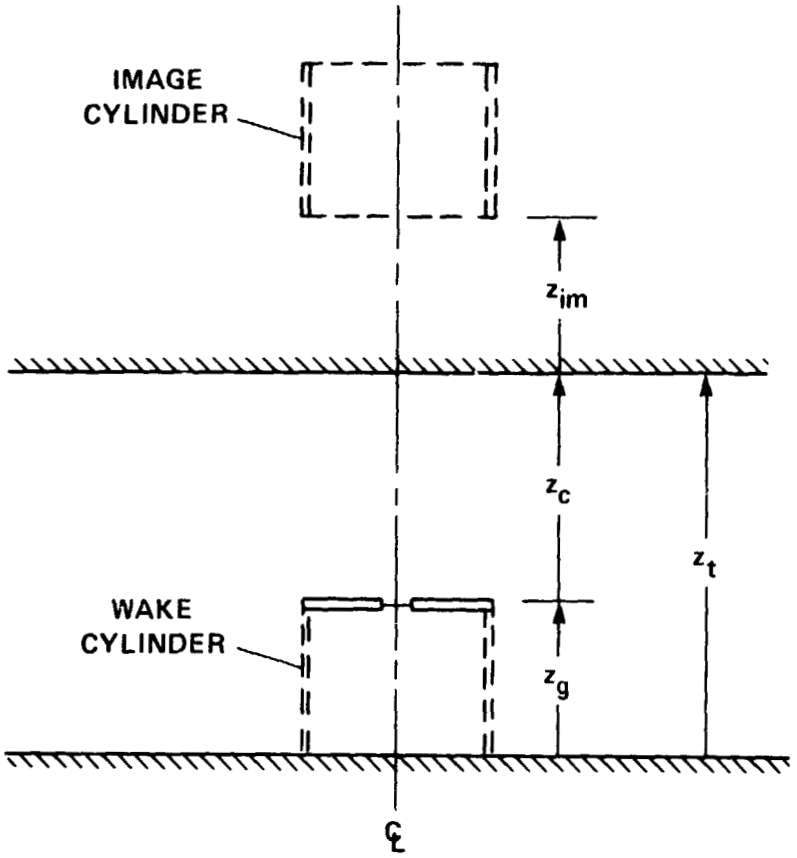

Figure 9.- Arrangement of two vortex cylinders used to represent wake of rotor and effect of ceiling and ground plane: $z_{im} = 5z_c^{1.25}$.

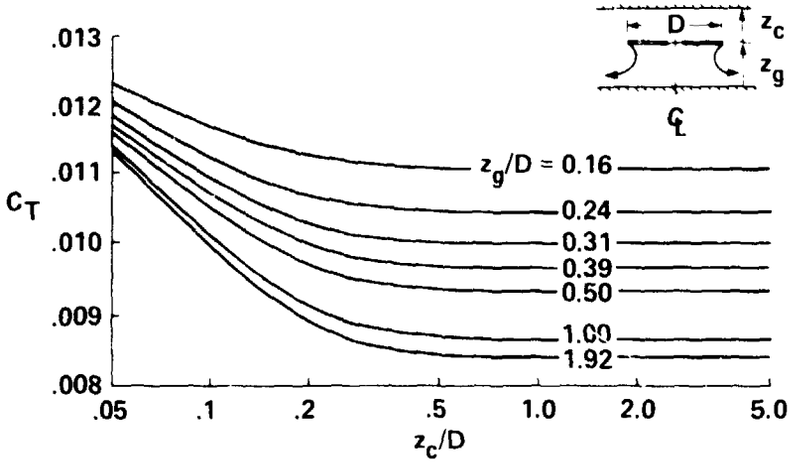

Figure 10.- Thrust coefficients predicted by theory that uses approximate image system: $C_L = 0.08\alpha_e - 0.00006\alpha_e^3$; $\alpha_b = 11.6° \pm 0.1°$.

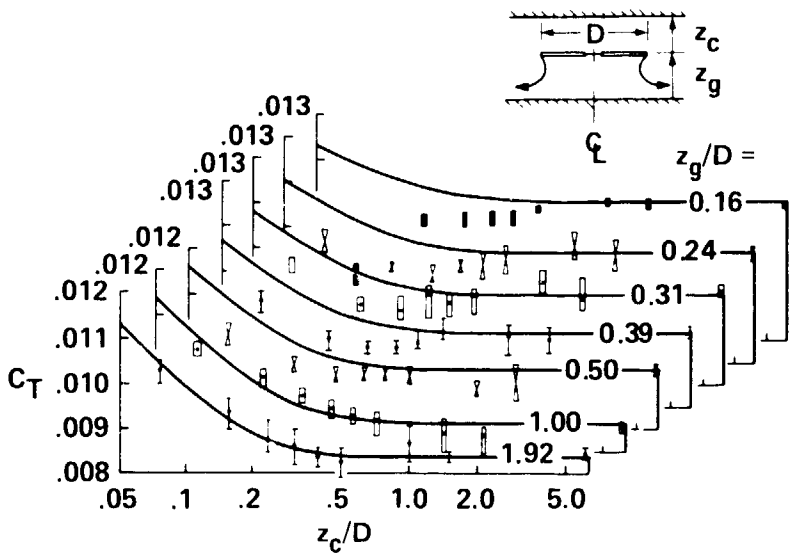

Figure 11.- Comparison of thrust measured on 0.324-m-diam (12.75-in.) rotor with values predicted by theory based on approximate image system; vertical length of symbols indicates excursions observed in C_T.

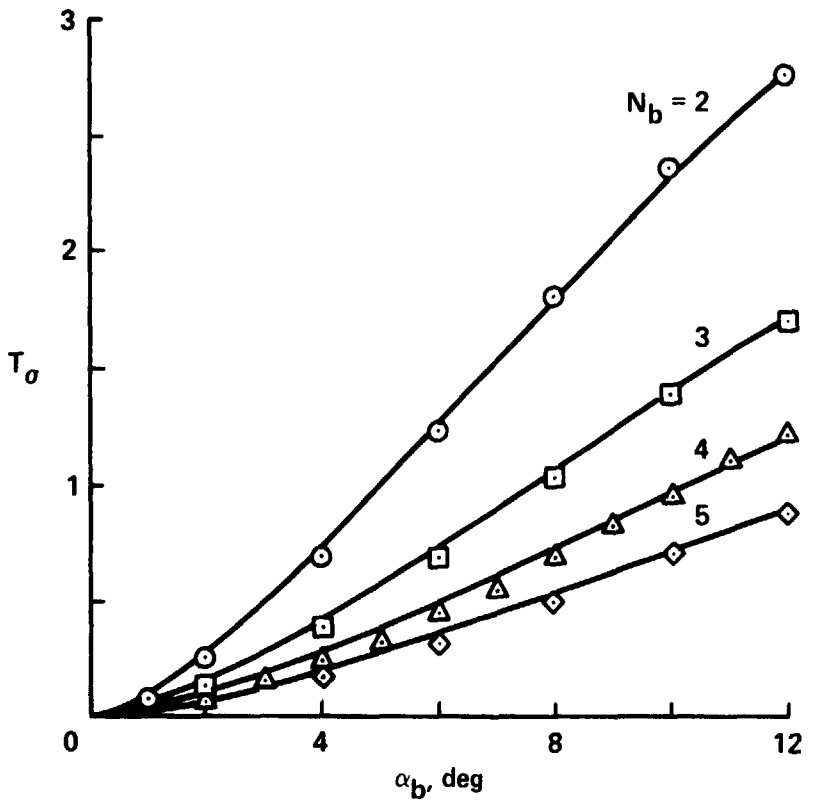

Figure 12.- Experimental thrust data (symbols) taken with no nearby boundaries by Knight and Hefner (ref. 2) on 1.5-m-diam (5-ft) rotors that have different numbers of blades N_b and geometric blade angles α_b; data are compared with theory (solid lines) that assumes $C_L = 0.1\alpha_e - 0.00002\alpha_e^4$ ($C_L = 0.8$ when $\alpha_e \geq 10°$) as lift-curve equation for the rotor blade sections.

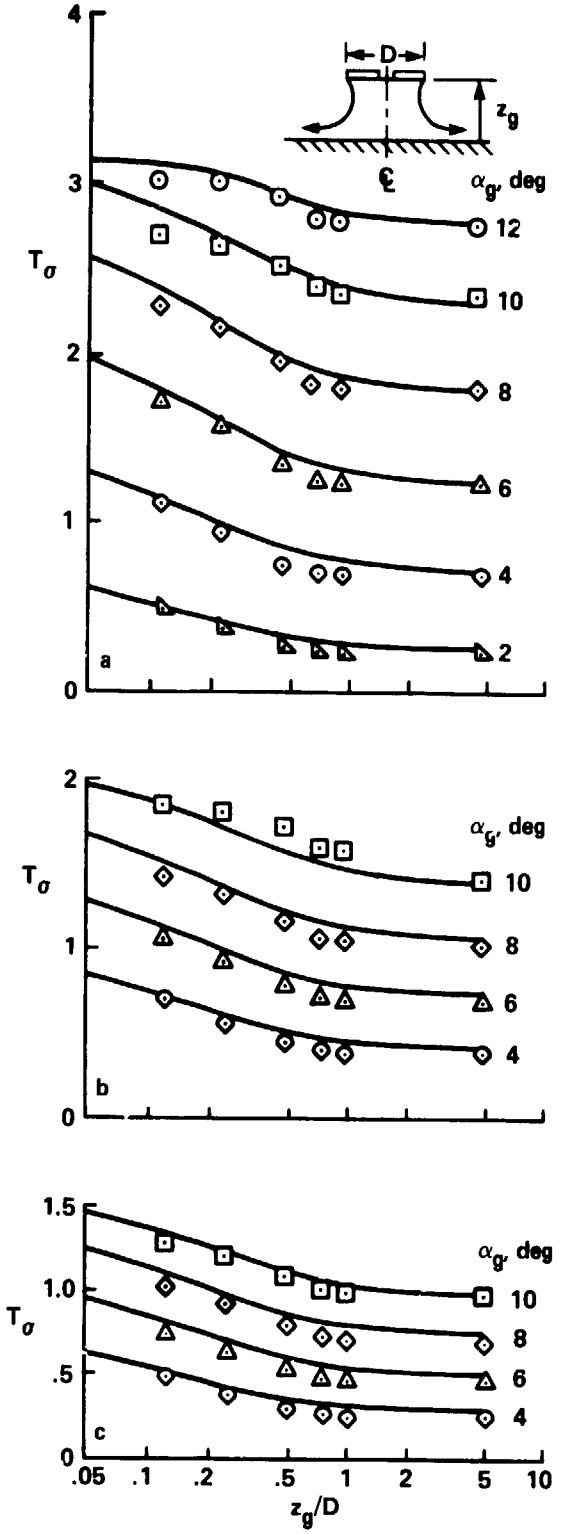

Figure 13.- Experimental thrust data (symbols) taken by Knight and Hefner (ref. 3) on 1.5-m-diam (5-ft) rotors in ground effect, using different geometric blade angles α_b and blade numbers N_b; data are compared with approximate theory (solid lines) which assumes $C_L = 0.1\alpha_e - 0.00002\alpha_e^4$ ($C_L = 0.8$ when $\alpha_e \geq 10°$) as lift-curve equation for the rotor blade sections: (a) Two-bladed rotor; (b) three-bladed rotor; (c) four-bladed rotor.

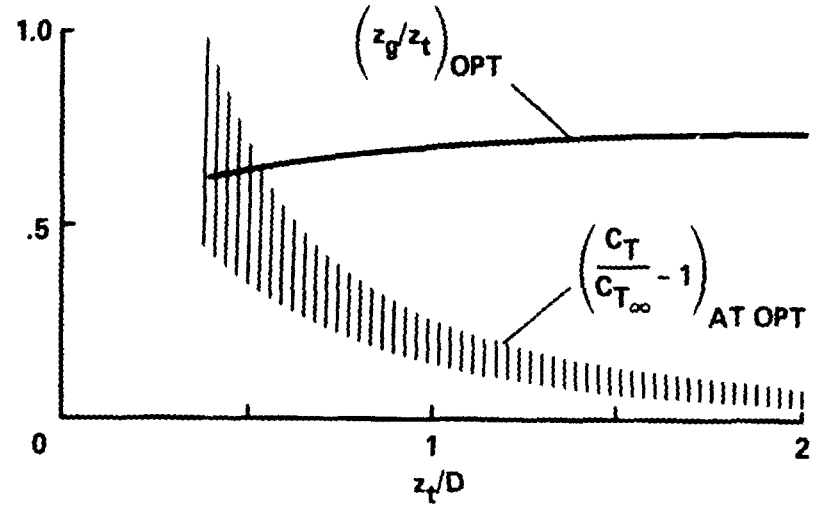

Figure 14.- Location of rotor disk between ground and ceiling planes at which total interference is a minimum for a range of tunnel heights: $z_t/D = (z_g + z_c)/D$. Also shown is predicted range of thrust change due to interference at optimum location; an off-optimum location usually causes no more than a 4% additional thrust increment.

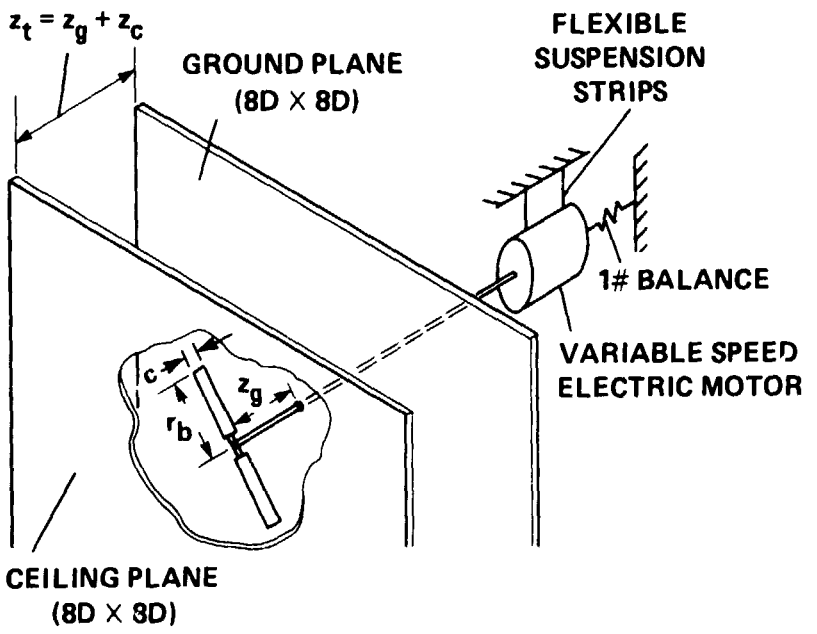

Figure 15.- Schematic of test setup: r_b = 16.2 cm (6.38 in.), c = 2.65 cm (1.04 in.).

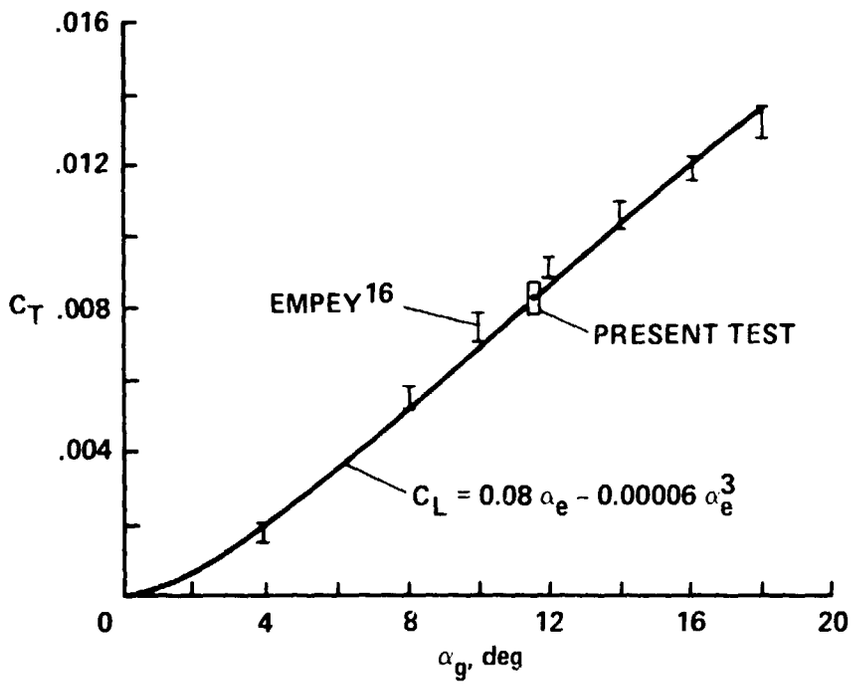

Figure 16.- Comparison of thrust measured on small rotor [D = 0.324-m (12.75 in.)] when no boundaries are nearby with data of Empey and Ormiston (ref. 16) and with theory. Theory computes thrust using $C_L = 0.08\alpha_e - 0.00006\alpha_e^3$ as lift-curve equation for the rotor-blade sections.

1 Report No.	2 Government Accession No.	3 Recipient's Catalog No
NASA TM 86754		

4 Title and Subtitle	5 Report Date
EFFECT OF GROUND AND/OR CEILING PLANES ON THRUST OF ROTORS IN HOVER	July 1985
	6 Performing Organization Code
7 Author(s)	8 Performing Organization Report No
Vernon J. Rossow	85256
	10 Work Unit No
9 Performing Organization Name and Address	
NASA Ames Research Center Moffett Field, CA 94035	11 Contract or Grant No
	13 Type of Report and Period Covered
12 Sponsoring Agency Name and Address	Technical Memorandum
National Aeronautics and Space Administration Washington, DC 20546	14 Sponsoring Agency Code 505-31-21

15 Supplementary Notes

Point of contact: Vernon J. Rossow, Ames Research Center, MS 247-1, Moffett Field, CA 94035, (914) 694-6681 or FTS 464-6681

16 Abstract

The thrust produced by a helicopter rotor hovering near ground and/or ceiling planes is investigated experimentally and theoretically. In the experiment, the thrust was measured on a 0.324-m-diam rotor operating between floor and ceiling planes which were located from 6 to 0.08 diam from the rotor disk. In the first theoretical model studied, the incompressible and inviscid flow induced by a sequence of vortex cylinders, located above and below the rotor to simulate the rotor wake and its interaction with the floor and ceiling planes, was considered. Comparison with experiment showed that this model overpredicts the change in thrust caused by the proximity of the walls. Therefore, a second arrangement of vortex cylinders was introduced which provides a more accurate prediction of the ground and ceiling effects on the thrust of the rotor in hover. The applicability of these results to a vented wind tunnel is also discussed.

17 Key Words (Suggested by Author(s))	18 Distribution Statement
Rotor testing Wind tunnel wall interference Aerodynamics	Unlimited Subject category - 02

19 Security Classif. (of this report)	20 Security Classif (of this page)	21 No of Pages	22 Price*
Unclassified	Unclassified	41	A03

*For sale by the National Technical Information Service, Springfield, Virginia 22161